

PRECONDITIONERS BASED ON VORONOI QUANTIZERS OF RANDOM VARIABLE COEFFICIENTS FOR STOCHASTIC ELLIPTIC PARTIAL DIFFERENTIAL EQUATIONS

NICOLAS VENKOVIC ^{*}, PAUL MYCEK [†], OLIVIER P. LE MAÎTRE [‡], AND LUC
GIRAUD [§]

Abstract. A preconditioning strategy is proposed for the iterative solve of large numbers of linear systems with variable matrix and right-hand side which arise during the computation of solution statistics of stochastic elliptic partial differential equations with random variable coefficients sampled by Monte Carlo. Building on the assumption that a truncated Karhunen-Loève expansion of a known transform of the random variable coefficient is known, we introduce a compact representation of the random coefficient in the form of a Voronoi quantizer. The number of Voronoi cells, each of which is represented by a centroidal variable coefficient, is set to the prescribed number P of preconditioners. Upon sampling the random variable coefficient, the linear system assembled with a given realization of the coefficient is solved with the preconditioner whose centroidal variable coefficient is the closest to the realization. We consider different ways to define and obtain the centroidal variable coefficients, and we investigate the properties of the induced preconditioning strategies in terms of average number of solver iterations for sequential simulations, and of load balancing for parallel simulations. Another approach, which is based on deterministic grids on the system of stochastic coordinates of the truncated representation of the random variable coefficient, is proposed with a stochastic dimension which increases with the number P of preconditioners. This approach allows to bypass the need for preliminary computations in order to determine the optimal stochastic dimension of the truncated approximation of the random variable coefficient for a given number of preconditioners.

Key words. Stochastic PDEs, Iterative methods, Preconditioners, Voronoi quantizers, Uncertainty quantification.

1. Introduction. Elliptic partial differential equations (PDEs), such as the steady-state heat equation, are prevalent in modeling numerous phenomena in physics, engineering, biology, and economics. Many of these phenomena exhibit inherent randomness, which propagates to quantities of interest. Consequently, realistic modeling efforts increasingly call for proper uncertainty quantification. However, in practical applications, the precise assessment of solution uncertainty, even for elliptic equations, necessitates the use of statistical estimators that rely on large computational models. While the randomness of stochastic PDEs can originate from multiple sources such as boundary conditions or a forcing term, the most challenging situation arises when the coefficients of the PDE are both random and variable. To this day, the development of novel methods to enhance the computational performance associated with uncertainty quantification in stochastic PDEs remains an active field of research, including, notably, elliptic equations. This work addresses the same crucial question, aiming to contribute to the ongoing efforts in advancing practical capabilities in modeling complex systems with inherent randomness, particularly stochastic elliptic PDEs with random variable coefficients.

Two types of methods are well-known and used to compute solution statistics of stochastic elliptic PDEs with random variable coefficients: methods based on a functional representation of the random solution, and simulation-based methods. The first type of methods consists of approximating the functional dependency of the random

^{*}NXP Semiconductors, Toulouse, France (venkovic@gmail.com).

[†]Cerfacs, Toulouse, France (mycek@cerfacs.fr).

[‡]CNRS, CMAP, École Polytechnique, Palaiseau, France (olivier.le-maitre@polytechnique.edu).

[§]HiePACS, Inria Bordeaux, Sud-Ouest, Talence, France (luc.giraud@inria.fr).

solution (or another quantity of interest) on the random coefficient. This includes spectral methods [23, 32], which have been widely applied to both linear and nonlinear PDEs with random variable coefficients [16, 33, 19, 28, 1, 41, 40]. The primary challenge with spectral methods lies in the dependence of the complexity associated with solving the coefficients of the functional representation on the number of random variables used for the stochastic discretization of the random variable coefficient. To mitigate the challenge posed by this curse of dimensionality, one approach involves leveraging dependencies by deriving low-rank representations using suitable tensor formats (for elliptic problems, refer to [42, 43, 44, 4, 3, 56, 12]). Meanwhile, additional efforts were deployed to enhance convergence and reduce the runtime associated with solving for the coefficients of the functional representation in the case of intrusive methods [31, 49, 34, 17]. On the other hand, non-intrusive methods rely on sampled realizations of the model solution. Examples include regression methods [7] and spectral projection methods [48, 50, 14, 15]. The second type of methods involves constructing statistical estimators which rely on sample solutions of the PDE computed for specific realizations of the variable coefficient [10, 36]. The main issue with simulation-based methods is the low convergence rate of these statistical estimators which, prompting efforts to alleviate this challenge. In particular, multilevel Monte Carlo methods [13] have proven effective in building estimators with better convergence properties at a given computational cost. Another way to improve simulation-based methods is by accelerating the convergence of the deterministic iterative linear solves conducted to obtain each solution realization. To this end, stochastic preconditioners based on non-overlapping domain decomposition were recently proposed so as to significantly enhance the convergence of the iterative linear solve of deterministic Schur complement systems [51]. In this work, we also aim at enhancing the preconditioning for large numbers of iterative linear solves conducted during the application of simulation-based methods. In particular, we introduce a straightforward, intuitive and embarrassingly parallelizable preconditioning strategy. This strategy leverages a functional representation of the random variable coefficient to construct compact representations of the coefficient. These representations take the form of a Voronoi quantizer, where centroids are employed to assemble a fixed number of deterministic preconditioners. These preconditioners are subsequently used to solve the linear systems, each one associated with a realization of the coefficient that is closest to the corresponding centroid.

The document is organized as follows. First, we provide a loose statement of the problem. Second, we introduce the preconditioning strategies proposed in this work and highlight their connection to finite-dimensional quantizers. Next, in Sections 4 through 6, we outline different methods for constructing such finite-dimensional quantizers. Finally, we explore specific features of the various preconditioning strategies and examine their impact on the convergence of iterative solves. Concluding remarks are then provided.

2. Problem statement. Consider a measurable space (Θ, Σ) with σ -algebra Σ rich enough to support all the random variables we encounter, along with the set Θ of outcomes θ . Let also $\Omega \subset \mathbb{R}^d$ be an open domain bounded by $\partial\Omega$ with $d \geq 1$. We are interested in computing statistics of the solution $u(\cdot, \theta)$ such that

$$(2.1) \quad \mathcal{L}(\kappa(x, \theta)) u(x, \theta) = f(x, \theta) \quad \forall x \in \Omega$$

$$(2.2) \quad u(x, \theta) = g(x, \theta) \quad \forall x \in \partial\Omega$$

is almost surely satisfied for $\theta \in \Theta$ and where \mathcal{L} is an elliptic operator in Ω which depends on the random variable coefficient $\kappa(\cdot, \theta)$. We assume that the random variable coefficient $\kappa(\cdot, \theta)$, as well as the forcing term $f(\cdot, \theta)$ and boundary condition $g(\cdot, \theta)$, are defined such that unique solutions to the stated problem exist. Conditions for the existence and uniqueness of solutions to stochastic elliptic PDEs can be found in [38]. Here, the only explicit, but non-sufficient assumption made about the random variable coefficient is that the realization $\kappa(\cdot, \theta)$ is almost surely square integrable, i.e., $\Pr[\kappa(\cdot, \theta) \in L^2(\Omega)] = 1$, where

$$(2.3) \quad L^2(\Omega) := \left\{ h : \Omega \rightarrow \mathbb{R} \mid \int_{\Omega} h(x)^2 \, dx < \infty \right\}.$$

For each $\theta \in \Theta$, a discretization of the elliptic operator is introduced such that an approximate solution $u^h(\cdot, \theta)$ in Ω is obtained by solving a linear system

$$(2.4) \quad \mathbf{A}(\theta)\mathbf{u}(\theta) = \mathbf{b}(\theta)$$

where $\mathbf{A}(\theta)$ is almost surely contained in $\text{GL}(n, \mathbb{R})$, i.e., the space of non-singular n -dimensional square matrices with real components. Sometimes, we express the discretized operator $\mathbf{A}(\theta)$ as a function of a deterministic variable coefficient, i.e., $\mathbf{A}(\kappa)$, in which case it should be understood that κ lies in some functional subspace which we loosely define as $\mathcal{A} : \Omega \rightarrow \mathbb{R}$.

This work focuses on the iterative solve of Eq. (2.4) for large numbers of $\theta \in \Theta$. For each such θ , an initial approximation $\mathbf{u}^{(0)}(\theta)$ of $\mathbf{u}(\theta)$ is set, and a sequence of iterates $\mathbf{u}^{(1)}(\theta), \dots, \mathbf{u}^{(j)}(\theta)$ which converges to $\mathbf{u}(\theta)$ is generated. Fixed-point, multigrid and Krylov subspace methods are common examples of such approaches. Depending on the properties of the discretized operator $\mathbf{A}(\theta)$, different Krylov subspace methods can be used, the most common of which being the generalized minimal residual algorithm, referred to as GMRES [53], the minimum residual method, referred to as MINRES [47], and the conjugate gradient algorithm [26]. See [52] for detailed presentations and application cases of these methods. Irrespective of the method used, we denote by $J(\theta)$ the smallest number j of iterations such that $\|\mathbf{A}(\theta)\mathbf{u}^{(j)}(\theta) - \mathbf{b}(\theta)\|_2 < \epsilon\|\mathbf{b}(\theta)\|_2$ for some $\epsilon > 0$. In other words, $J(\theta)$ is the number of necessary solver iterations to reach a normwise backward error of ϵ . One means to accelerate the convergence of such iterative methods is the use of a preconditioner, i.e., $\mathbf{M}(\theta) \in \text{GL}(n, \mathbb{R})$ such that $\mathbf{v} \in \mathbb{R}^n \mapsto \mathbf{M}(\theta)^{-1}\mathbf{v}$ can be computed efficiently while $\mathbf{M}(\theta)$, which needs not be known explicitly, is a good approximation of $\mathbf{A}(\theta)$. The aim of this work is to define such a mapping $\mathbf{v} \in \mathbb{R}^n \mapsto \mathbf{M}(\theta)^{-1}\mathbf{v}$ so that $J(\theta)$ is minimized for large numbers of θ . Typically, a good preconditioner is such that $J(\theta) \ll n$ irrespective of θ .

3. Preconditioning strategies. Let us define preconditioning strategies as consisting of both

1. A *P-quantizer* $q : \kappa \in \mathcal{A} \mapsto \hat{\kappa} \in \hat{\mathcal{A}}$ with centroidal variable coefficients given by the elements of a codebook $\hat{\mathcal{A}} := \{\hat{\kappa}_p \in \mathcal{A}, p = 1, \dots, P\}$. The aim of q is to serve as a compact representation of the random variable coefficient—see [21, 24, 35] for references on vector quantization, and [30, 18] for extensions to Hilbert and Banach function spaces.
2. A *preconditioner* $\mathbf{M} : \kappa \in \mathcal{A} \mapsto \mathbf{M}(\kappa) \in \text{GL}(n, \mathbb{R})$. Then, we are interested in the composition $\mathbf{M} \circ q : \kappa \in \mathcal{A} \mapsto \hat{\mathbf{M}} \in \{\hat{\mathbf{M}}_1, \dots, \hat{\mathbf{M}}_P\}$. The preconditioners $\hat{\mathbf{M}}_1, \dots, \hat{\mathbf{M}}_P$ may consist of factorizations of the discretized operators of the centroidal variable coefficients, in which case we have $\hat{\mathbf{M}}_p := \mathbf{A}(\hat{\kappa}_p)$ for $p =$

$1, \dots, P$. Other possible choices are: solving cycles of algebraic multigrids of $\mathbf{A}(\hat{\kappa}_p)$, in which case $\hat{\mathbf{M}}_p$ needs not even be known as long as one can evaluate $\mathbf{v} \in \mathbb{R}^n \mapsto \hat{\mathbf{M}}_p^{-1}\mathbf{v}$; block Jacobi (bJ), i.e., factorizations of diagonal blocks of $\mathbf{A}(\hat{\kappa}_p)$; domain decomposition and so forth. See [52] for more suggestions.

We assume there exists an invertible transport map $T : L^2(\Omega) \rightarrow L^2(\Omega)$ such that $T^{-1}\kappa$ has zero mean and is a second order random field which admits a Karhunen-Loève (KL) expansion. In order to introduce the KL expansion of $T^{-1}\kappa$, we must know the covariance function $C : \Omega \times \Omega \rightarrow \mathbb{R}$ given by $(x, x') \mapsto \mathbb{E}[T^{-1}\kappa(x)T^{-1}\kappa(x')]$. Moreover, we assume that the kernel C is such that the integral operator $h \in L^2(\Omega) \mapsto \int_{\Omega} C(x, \cdot)h(x)dx$ is symmetric and positive semi-definite. Then, the eigen-pairs $(\lambda_k, \Phi_k) \in \mathbb{R} \times L^2(\Omega)$ of the operator are such that

$$(3.1) \quad \int_{\Omega} \int_{\Omega} C(x', x)\Phi_k(x')dx'v(x)dx = \lambda_k \int_{\Omega} \Phi_k(x)v(x)dx \quad \forall v \in L^2(\Omega)$$

with $\langle \Phi_k, \Phi_{\ell} \rangle_{\Omega} = \delta_{k\ell}$ and $\lambda_1 \geq \lambda_2 \geq \dots \geq 0$, where $\langle h, \ell \rangle_{\Omega}$ is the $L^2(\Omega)$ inner product

$$(3.2) \quad \langle h, \ell \rangle_{\Omega} := \int_{\Omega} h(x)\ell(x)dx \quad \forall h, \ell \in L^2(\Omega)$$

with induced norm

$$(3.3) \quad \|h\|_{\Omega}^2 = \langle h, h \rangle_{\Omega} = \int_{\Omega} h(x)^2 dx.$$

The random field $T^{-1}\kappa$ can then be expressed as

$$(3.4) \quad T^{-1}\kappa(x, \theta) = \sum_{k=1}^{\infty} \lambda_k^{1/2} \Phi_k(x) \xi_k(\theta)$$

where ξ_1, ξ_2, \dots are uncorrelated random variables. In the special case where $T^{-1}\kappa$ is a Gaussian process, the random variables are independent and identically distributed standard normal. By only using the m dominant eigen-pairs $(\lambda_1, \Phi_1), \dots, (\lambda_m, \Phi_m)$ such that $\lambda_1 \geq \dots \geq \lambda_m > 0$, we can approximate $T^{-1}\kappa$ with

$$(3.5) \quad \hat{T}_m^{-1}\kappa(x, \theta) := \sum_{k=1}^m \lambda_k^{1/2} \Phi_k(x) \xi_k(\theta)$$

where ξ_1, \dots, ξ_m are the components of the m -dimensional random vector $\boldsymbol{\xi}$ with probability measure $\mu_{\boldsymbol{\xi}}$. We denote the underlying representation error by

$$(3.6) \quad \epsilon(\hat{T}_m^{-1}\kappa) := \mathbb{E}[\|\hat{T}_m^{-1}\kappa - T^{-1}\kappa\|_{\Omega}^2].$$

Let us assume that $T^{-1}\kappa(x)$ has a stationary variance denoted by σ^2 and that the eigen-pairs $(\lambda_k, \Phi_k) \in \mathbb{R}^+ \times L^2(\Omega)$ with $k = 1, \dots, m$ properly approximate the dominant eigen-pairs of C . Then, we have

$$(3.7) \quad \epsilon(\hat{T}_m^{-1}\kappa) = \sigma^2 - \sum_{k=1}^m \lambda_k.$$

For the design of quantizers, we introduce the projection

$$(3.8) \quad \hat{P}_m^{\leftarrow} : h \in L^2(\Omega) \mapsto \begin{bmatrix} \lambda_1^{-1/2} \langle \Phi_1, h \rangle_{\Omega} \\ \vdots \\ \lambda_m^{-1/2} \langle \Phi_m, h \rangle_{\Omega} \end{bmatrix} \in \mathbb{R}^m$$

as well as

$$(3.9) \quad \hat{P}_m^{\rightarrow} : \chi \in \mathbb{R}^m \mapsto \sum_{k=1}^m \lambda_k^{1/2} \chi_k \Phi_k(\cdot) \in L^2(\Omega).$$

Then, $T(\hat{P}_m^{\rightarrow}(\hat{P}_m^{\leftarrow}(T^{-1}\kappa(\cdot, \theta))))$ serves as an approximation of $\kappa(\cdot, \theta)$. Moreover, the use of \hat{P}_m^{\leftarrow} and \hat{P}_m^{\rightarrow} allows to substitute the quantization of κ , or more precisely of $\hat{T}_m^{-1}\kappa$, by a finite-dimensional problem. That is, we will be searching for a quantizer $q_2 : \eta \in \mathbb{R}^m \mapsto \hat{\eta} \in \hat{\mathcal{H}} \subset \mathbb{R}^m$ with a codebook $\hat{\mathcal{H}} := \{\hat{\eta}_1, \dots, \hat{\eta}_P\}$ for the random vector $T_2^{-1}(\xi)$, where the invertible map $T_2 : \mathbb{R}^m \rightarrow \mathbb{R}^m$ is introduced to allow some flexibility in the design of q_2 . For a given q_2 , we are interested in the quantizer

$$(3.10) \quad q : \kappa(\cdot, \theta) \in \mathcal{A} \mapsto \tilde{T}_m^{\rightarrow}(q_2(\tilde{T}_m^{\leftarrow}\kappa(\cdot, \theta))) \in \hat{\mathcal{A}} \subset \mathcal{A}$$

in which we made use of $\tilde{T}_m^{\rightarrow} := T \circ \hat{P}_m^{\rightarrow} \circ T_2$ and $\tilde{T}_m^{\leftarrow} := T_2^{-1} \circ \hat{P}_m^{\leftarrow} \circ T^{-1}$. Then, the application of a strategy consists of preconditioning the iterative solve of $\mathbf{A}(\theta)\mathbf{u}(\theta) = \mathbf{b}(\theta)$ with a preconditioner $\mathbf{M}(\theta) := \mathbf{M}(q(\kappa(\cdot, \theta)))$. To do so, there remains to design q_2 and to select a type of preconditioner.

3.1. Optimal preconditioning strategies. An optimal preconditioning strategy is one that somehow minimizes the iteration number J . In theory, one can define a quantizer \tilde{q} that maps every element of \mathcal{A} to itself. Then, a preconditioning strategy based on \tilde{q} with $\mathbf{M}(\theta) := \mathbf{A}(\kappa(\cdot, \theta))$ is such that $J(\theta) = 1$ almost everywhere in Θ . While being optimal, this solution has no practical use. The reasons are the following. First, computing a precise factorization of $\mathbf{A}(\theta)$ is at least as costly as solving $\mathbf{A}(\theta)\mathbf{u}(\theta) = \mathbf{b}(\theta)$. Second, computing or setting-up a preconditioner carries some computational and memory costs. Thus, P will be limited by practical considerations, namely, the total memory available for a simulation. P may be referred to as the rate of quantization, and we are interested in fixed rate quantization. Another matter of concern lies in the scheduling of computations. That is, when allocating resources for a simulation, one may not only want to minimize $\mathbb{E}[J]$, but also some higher order moments, or even to impose some distribution on J . A first step in these directions lies in the formulation of measurable information about J which statistically relates to the random variable coefficient and its quantizer.

Irrespective of the type of preconditioner used, the representation error of $\kappa(\cdot, \Theta)$ by $q(\kappa(\cdot, \Theta))$ is characterized by a distortion

$$(3.11) \quad w(q, d) := \mathbb{E}[d(\kappa, q(\kappa))] = \int_{\Theta} d(\kappa(\cdot, \theta), q(\kappa(\cdot, \theta))) d\mu(\theta)$$

where the distortion functional (or divergence) $d : \mathcal{A} \times \mathcal{A} \rightarrow [0, \infty)$ measures proximity between realizations of the variable coefficient. A loose definition of proximity allows, in principle, to recast a variety of functionals in the form of distortions. Given our objective to minimize the number of solver iterations J , we should aim at using divergences d such that minimizing $w(q, d)$ over all P -quantizers $q \in \mathcal{Q}_P$ allows to minimize some relevant information about J .

Let us denote by $\mathcal{V}_P \subset \mathcal{Q}_P$ the set of all Voronoi P -quantizers. That is, for all $q \in \mathcal{V}_P$, there exists $\hat{\mathcal{A}} := \{\hat{\kappa}_1, \dots, \hat{\kappa}_P\} \subset \mathcal{A}$ such that

$$(3.12) \quad q : \kappa \in \mathcal{A} \mapsto \sum_{p=1}^P \hat{\kappa}_p \mathbf{1}[\kappa \in \mathcal{A}_p]$$

where

$$(3.13) \quad \mathcal{A}_p \subseteq \{\kappa \in \mathcal{A}, d(\kappa, \hat{\kappa}_p) \leq d(\kappa, \hat{\kappa}_q), q = 1, \dots, P\}$$

is such that $\mathcal{A}_1, \dots, \mathcal{A}_P$ form a Borel partition of \mathcal{A} . We say that q is the $\hat{\mathcal{A}}$ -nearest projection. The advantage of Voronoi quantizers lies in that, for all pairs $(q, q') \in \mathcal{V}_P \times \mathcal{Q}_P$ of quantizers with the same codebook $\hat{\mathcal{A}}$, we have $w(q, d) \leq w(q', d)$. Therefore, in an attempt to minimize distortion, we rely on Voronoi quantizers.

Consider a Voronoi partition $\mathcal{A}_1, \dots, \mathcal{A}_P$ induced by a quantizer q with an unknown codebook $\hat{\mathcal{A}} := \{\hat{\kappa}_1, \dots, \hat{\kappa}_P\}$. We can then express the distortion as a functional of the codebook, i.e., $w(\hat{\mathcal{A}}, d)$. To do so, we define a conditional expectation operator $\mathbb{E}_p[\cdot] := \mathbb{E}[\cdot | \kappa \in \mathcal{A}_p]$ and an attribution frequency $f_p := \mu(\mathcal{A}_p)$ so that $\sum_{p=1}^P f_p = 1$. We also introduce the local distortion $w_p(q, d) := \mathbb{E}_p[d(\kappa, q(\kappa))]$ which we also express in terms of the centroidal coefficients, i.e., $w_p(\hat{\kappa}_p, d)$, so that

$$(3.14) \quad w(\hat{\mathcal{A}}, d) = \sum_{p=1}^P f_p w_p(\hat{\kappa}_p, d).$$

Then, the following can be shown [18]. If $f_p > 0$ and $\mathbb{E}_p[\kappa] \in ri(\mathcal{A})$ for $p = 1, \dots, P$, where $ri(\mathcal{A})$ denotes the relative interior of \mathcal{A} , then, in order to minimize $w(\hat{\mathcal{A}}, d)$, the codebook $\hat{\mathcal{A}} = \{\hat{\kappa}_1, \dots, \hat{\kappa}_P\}$ must be such that

$$(3.15) \quad \hat{\kappa}_p \in \arg \min_{\hat{\kappa} \in ri(\mathcal{A})} w_p(\hat{\kappa}, d)$$

for $p = 1, \dots, P$. That is, given a Voronoi partition, the distortion is minimized by selecting centroidal coefficients which are minimizers of local distortions.

Among all distortion functionals, we wish to consider those that allow for the minimization of Eq. (3.11) with respect to q . In particular, Bregman divergences [8] admit properties which allow to devise algorithms for the minimization of distortion in both finite [2], and infinite-dimensional spaces [18]. They can be defined as follows.

DEFINITION 3.1. *Let $\varphi : L^2(\Omega) \rightarrow \mathbb{R}$ be a strictly convex, twice-continuously Fréchet-differentiable functional. Then, a Bregman divergence is given by*

$$(3.16) \quad d_\varphi(\kappa, \kappa') = \varphi(\kappa) - \varphi(\kappa') - \delta\varphi(\kappa, \kappa' - \kappa) \quad \forall \kappa, \kappa' \in \mathcal{A},$$

where $\delta\varphi(\kappa, \kappa' - \kappa)$ denotes the Fréchet derivative of φ at κ in the direction of $\kappa' - \kappa$, see [20].

An important result of [2] was extended by [18] to the case of functional Bregman divergences. That is, for any Bregman divergence d_φ , if a (Borel) subset \mathcal{A}_p of \mathcal{A} is such that $f_p > 0$ and $\mathbb{E}_p[\kappa] \in ri(\mathcal{A})$, then, the local distortion $w_p(\hat{\kappa}, d_\varphi)$ reaches its infimum at a unique element of $ri(\mathcal{A})$, namely $\mathbb{E}_p[\kappa]$. A consequence of this result is that iterative algorithms such as k -means can be designed to approximate optimal quantizers that converge to local minima of distortion.

4. Computation of stationary quantizers. There exist several numerical methods for the computation of stationary vector quantizers. In particular, we consider L^2 stationary quantizers of $T_2^{-1}(\boldsymbol{\xi})$, which means that we aim at minimizing the distortion

$$(4.1) \quad w_2(q_2) := \mathbb{E}[\|T_2^{-1}(\boldsymbol{\xi}) - q_2(T_2^{-1}(\boldsymbol{\xi}))\|^2] = \int_{\Theta} \|T_2^{-1}(\boldsymbol{\xi}) - q_2(T_2^{-1}(\boldsymbol{\xi}))\|^2 d\mu_{\boldsymbol{\xi}}(\theta).$$

We let q_2 be Voronoi and we denote by $\mathcal{H}_1, \dots, \mathcal{H}_P$ the partition of $T_2^{-1}(\mathbb{R}^m)$ induced by q_2 . Then, we have

$$(4.2) \quad q_2(T_2^{-1}(\boldsymbol{\xi})) := \sum_{p=1}^P \hat{\boldsymbol{\eta}}_p \mathbf{1}[T_2^{-1}(\boldsymbol{\xi}) \in \mathcal{H}_p]$$

where $\hat{\boldsymbol{\eta}}_p = T_2^{-1}(\hat{\boldsymbol{\xi}}_p)$. The distortion can then be decomposed as follows into local contributions:

$$(4.3) \quad w_2(q_2) = \sum_{p=1}^P w_{2,p}(q_2) \mu_{\boldsymbol{\xi}}(T_2^{-1}(\mathcal{H}_p))$$

where $w_{2,p}(q_2) := \mathbb{E}[\|T_2^{-1}(\boldsymbol{\xi}) - q_2(T_2^{-1}(\boldsymbol{\xi}))\|^2 | T_2^{-1}(\boldsymbol{\xi}) \in \mathcal{H}_p]$. A P -quantizer q_2 is P -stationary if it is a critical point of $w_2 : \mathcal{Q}_P \rightarrow \mathbb{R}^+$ or, equivalently, the quantizer q_2 is Voronoi and such that $q_2(T_2^{-1}(\boldsymbol{\xi})) = \mathbb{E}[T_2^{-1}(\boldsymbol{\xi}) | q_2(T_2^{-1}(\boldsymbol{\xi}))]$. Obviously, an optimal P -quantizer is always P -stationary.

In practice, it is not tractable to measure with $\mu_{\boldsymbol{\xi}}$, and empirical measures need be introduced. That is, we are given an n_s -sample $\kappa_1, \dots, \kappa_{n_s}$ of independent and identically distributed observations of the random variable coefficient, and we compute $\boldsymbol{\xi}_s := \hat{P}_m^{\kappa}(T^{-1}\kappa_s)$ for $s = 1, \dots, n_s$. The distortion $w_2(q_2)$ is then approximated by

$$(4.4) \quad w_2^{(n_s)}(q_2) := \frac{1}{n_s} \sum_{s=1}^{n_s} \|T_2^{-1}(\boldsymbol{\xi}_s) - q_2(T_2^{-1}(\boldsymbol{\xi}_s))\|^2$$

which is also given by

$$(4.5) \quad w_2^{(n_s)}(q_2) = \sum_{p=1}^P f_{2,p}^{(n_s)} w_{2,p}^{(n_s)}(q_2)$$

where

$$(4.6) \quad f_{2,p}^{(n_s)} = \frac{1}{n_s} \sum_{s=1}^{n_s} \mathbf{1}[T_2^{-1}(\boldsymbol{\xi}_s) \in \mathcal{H}_p]$$

is the empirical measure of \mathcal{H}_p associated with $\boldsymbol{\xi}_1, \dots, \boldsymbol{\xi}_{n_s}$, and

$$(4.7) \quad w_{2,p}^{(n_s)}(q_2) = \frac{1}{f_{2,p}^{(n_s)} n_s} \sum_{s=1}^{n_s} \|T_2^{-1}(\boldsymbol{\xi}_s) - q_2(T_2^{-1}(\boldsymbol{\xi}_s))\|^2 \mathbf{1}[T_2^{-1}(\boldsymbol{\xi}_s) \in \mathcal{H}_p].$$

Different iterative methods exist to compute finite dimensional stationary quantizers q_2 on the basis of those empirical quantities. In particular, the k -means algorithm, sometimes referred to as Lloyd's method [27, 54], and the competitive learning vector quantization (CLVQ) algorithm [45] are perhaps the most used approaches for this task. Here, we provide a short description of these two methods along with a brief mention of other documented approaches. For more detailed descriptions and algorithms, we refer the reader to Section 4.3 of [57].

4.1. k -means. The term k -means was first used by MacQueen in 1967 [39], though the idea goes back to Steinhaus in 1956 [55]. The standard algorithm was first proposed by Lloyd of Bell Labs in 1957 as a technique for pulse-code modulation, although it was not published as a journal article until 1982 [37]. The algorithm works as follows. Given an initial codebook $\hat{\mathcal{H}}^{(0)}$ for a P -quantizer of $T_2^{-1}\xi$, alternate between the two following steps. First, compute the Voronoi partition induced by the codebook for a given Bregman divergence. Second, re-calculate the centroidal fields of the codebook as the conditional expectations of the new Voronoi partition. The k -means algorithm converges, but slowly for large values of the dimension m . It attempts to solve an NP-hard problem, even for low values of m , at a cost of $\mathcal{O}(n_s P)$ FLOPs per iteration.

4.2. Competitive learning. It is often argued (see [45]) that Lloyd’s method, i.e., k -means, is untractable in multiple dimensions, i.e., when m becomes large. Hence, approaches based on learning algorithms are favored when m is large so as to yield better results, see [29] for an example in automatic classification. In particular, we consider the CLVQ algorithm (see [58] or [6]) which is used by Pagès and Printemps [46] for the quantization of Gaussian RVs, as well as by Pagès [45] for numerical integration. The algorithm works as follows. First, the competitive phase of the method is the most consuming because it uses a nearest neighbor search at each step to find the nearest centroid in the codebook to the randomly generated vector. The second phase, called the learning phase, updates the nearest centroid of the quantizer by a homothety.

4.3. Other methods. Several other methods exist to reach estimators of stationary vector quantizers, see [11] for a list of methods applied to color quantization (i.e., with $m = 3$). In particular, we mention the following approaches. First, the octree method [22] is a two-phase method that starts by building an octree (a tree data structure in which each internal node has up to eight children) that represents the vector distribution of the input data \mathcal{H} and then, starting from the bottom of the tree, prunes the tree by merging its nodes until P vectors are obtained. Second, the modified minmax method [59] chooses the first centroid $\hat{\eta}_1^{(0)}$ arbitrarily from the data set \mathcal{H} and the p -th centroid $\hat{\eta}_p^{(0)}$ with $p \in \{2, \dots, P\}$ is chosen to be the point that has the largest minimum weighted L^2 distance to the previously selected centroids $\hat{\eta}_1^{(0)}, \dots, \hat{\eta}_{p-1}^{(0)}$. Each of these initial centroids is then recalculated as the mean of the vectors assigned to it. Third, the split & merge method [9] has two phases. First, the data set \mathcal{H} is partitioned uniformly into $B > P$ clusters. This initial set of partitions is represented as an adjacency graph. In the second phase, $B - P$ merge operations are performed to obtain the final P clusters. At each step of the second phase, the pair of clusters with the minimum joint quantization error are merged.

5. Quantizations based on deterministic grids. Until now, we focused on the design of P -quantizers using an independent number m of dominant modes of a truncated KL expansion with a corresponding representation error $\epsilon(\hat{T}_m^{-1}\kappa)$. However, some preliminary experiments we conducted have shown that, depending on the number P of preconditioners wanted, considering all the modes available for the approximation of the random coefficient in the design of a quantizer, i.e., letting $m = n_{\text{KL}}$, does not always yield smaller average numbers of solver iterations. Therefore, in order to more efficiently impact the preconditioning strategy, it is better to limit the number of dominant modes considered for the quantization based on the number of preconditioners. That is, the number m of dominant modes considered

should depend on the number P of preconditioners. One way to establish a dependence of the number of dominant modes on the number of preconditioners is to resort to deterministic grids. In particular, we consider deterministic grids whose design is specified through a scalar grid parameter $s > 0$. The independent variable of those designs is the number m of dominant modes such that $1 \leq m \leq n_{\text{KL}}$ and for which we have $P = 1 + 2^m$. To indicate the number of dominant modes of the KL expansion considered for the quantization, we resort to the notation $q_2^{(m)}$ where m is the number of modes. In particular, for $m = 1$, we use

$$(5.1) \quad q_2^{(1)}(\xi) := T_2^{-1}(0)\mathbf{1}[-s/2 \leq \xi < s/2] + T_2^{-1}(-s)\mathbf{1}[\xi < s/2] + T_2^{-1}(s)\mathbf{1}[s/2 \leq \xi]$$

so as to provide a symmetric solution with $P = 3$. In order for $q_2^{(1)}$ to yield a partition with constant attribution frequencies, we let $s := 2F^{-1}(2/3) \approx 0.8614$. In higher dimensions, i.e., for $m > 1$, we have

$$(5.2) \quad q_2^{(m)}(\xi) = \sum_{p=0}^{2^m} T_2^{-1}(\hat{\xi}_p)\mathbf{1}[T_2^{-1}(\xi) \in \mathcal{H}_p]$$

where $\mathcal{H}_0, \dots, \mathcal{H}_{2^m}$ form a Voronoi partition of $T_2^{-1}(\mathbb{R}^m)$ and are given such that

$$(5.3) \quad \mathcal{H}_p \subseteq \left\{ T_2^{-1}(\xi), \xi \in \mathbb{R}^m, \|\xi - \hat{\xi}_p\| \leq \|\xi - \hat{\xi}_q\|, q = 0, \dots, 2^m \right\}$$

in which $\hat{\xi}_0 := \mathbf{0}$ and $\hat{\xi}_1, \dots, \hat{\xi}_{2^m}$ denote the vertices of the centered and aligned m -dimensional hypercube of side length $2s$. The same value of grid parameter s is considered for all values of m .

6. Choice of map T_2 . The choice of the map T_2 bears important consequences on the design of the stationary quantizer q_2 . Here, we present two choices of maps, namely, one which leads to the minimization of the $L^2(\Omega)$ -distortion of $\hat{T}_m^{-1}\kappa$, and another which aims at producing constant attribution frequencies.

6.1. Minimizing the $L^2(\Omega)$ -distortion of an induced quantizer of $\hat{T}_m^{-1}\kappa$. By invoking the orthonormality of the eigenfunctions Φ_1, \dots, Φ_m along with Eq. (3.5), we can show that

$$(6.1) \quad \|\hat{T}_m^{-1}\kappa(\cdot, \theta)\|_{\Omega}^2 = \sum_{k=1}^m \lambda_k \xi_k(\theta)^2 = \xi(\theta)^T \mathbf{\Lambda} \xi(\theta) = \|\mathbf{\Lambda}^{1/2}(\xi(\theta))\|^2.$$

That is, the map

$$(6.2) \quad T_2^{-1} : \chi \mapsto \mathbf{\Lambda}^{1/2} \chi$$

is such that

$$(6.3) \quad \|T_2^{-1}(\xi(\theta))\|^2 = \|\hat{T}_m^{-1}\kappa(\cdot, \theta)\|_{\Omega}^2.$$

Consequently, the design of a quantizer q_2 which minimizes the L^2 -distortion of a compact representation of $T_2^{-1}(\xi)$ is then such that the quantizer $\hat{P}_m^{\rightarrow} \circ T_2 \circ q_2 \circ T_2^{-1} \circ \hat{P}_m^{\leftarrow}$ minimizes the $L^2(\Omega)$ -distortion of the induced compact representation of $\hat{T}_m^{-1}\kappa$.

6.2. Quantizers with constant attribution frequencies. The second choice of map, which aims at producing stationary quantizers with constant attribution frequencies, is

$$(6.4) \quad T_2^{-1} : \chi \mapsto \mathbf{A}^{1/2} F_\xi \circ \chi \quad \text{where} \quad F_\xi \circ \chi = \begin{bmatrix} F_\xi(\chi_1) \\ \vdots \\ F_\xi(\chi_m) \end{bmatrix}$$

in which $F_\xi(\chi) = \Pr[\xi \leq \chi]$ in the case where $T^{-1}\kappa$ is a Gaussian process.

6.3. Effect on load balancing. We wish to characterize the effect of choosing either of these two maps T_2 on the load balancing of a Monte Carlo simulation. In particular, we want to know how the time taken to solve all the linear systems attributed to a Voronoi cell varies across the quantization. For a given cell, this time is well accounted for by the cumulated number of solver iterations

$$(6.5) \quad \Sigma_{J(\hat{\Theta}_p)} = \sum_{\theta \in \hat{\Theta}_p} J(\theta)$$

where $\hat{\Theta}_p$ is the set of all the realizations of the linear systems preconditioned by $\hat{\mathbf{M}}_p$. The sets $\hat{\Theta}_1, \dots, \hat{\Theta}_P$ form a partition of the finite subset $\hat{\Theta} \subset \Theta$ of realizations for a given simulation. Then, the distribution of $\Sigma_{J(\hat{\Theta}_p)}$ as a function of p serves as a detailed representation of process activity.

7. Numerical experiments. Some experiments are conducted in order to better understand some aspects of the methods presented in this work. In particular, some of the experiments require the consideration of a specific PDE. For those, we consider the isotropic Poisson equation with a random variable coefficient defined in a unit square along with deterministic homogeneous boundary conditions and a unit forcing term. That is, we aim at finding $u : \Omega \times \Theta \rightarrow \mathbb{R}$ such that

$$(7.1) \quad \nabla \cdot [\kappa(x, \theta) \nabla u(x, \theta)] = 1 \quad \forall x \in \Omega$$

$$(7.2) \quad u(x, \theta) = 0 \quad \forall x \in \partial\Omega$$

is almost surely satisfied in a weak sense over $\Omega := (0, 1)^2$. The discretization scheme used is a Galerkin projection over the space $V \subset L^2(\Omega)$ spanned by the basis functions ϕ_i of the \mathbb{P}_1 finite elements of an unstructured triangular mesh. Consequently, the discretized operator $\mathbf{A}(\theta)$ is almost surely symmetric positive definite (SPD) so that we can use a preconditioned conjugate gradient (PCG) algorithm [52] as the iterative solver of choice.

The same discretization scheme is used for the computation of truncated KL expansions of the zero-mean Gaussian process $G := T^{-1}\kappa$ with $T := \log$ so that κ is a log-normal variable coefficient. We further assume that G is stationary with squared exponential covariance, unit variance and correlation length of 0.1. That is, we have $C(x, x') := \mathbb{E}[G(x, \cdot)G(x', \cdot)] = \exp(-(x-x')^T(x-x')/(0.1)^2)$ for all $x, x' \in \Omega$. Then, given that $T^{-1}\kappa$ is a Gaussian process, ξ_1, ξ_2, \dots are independent identically distributed standard Gaussian random variables.

The following experiments are conducted. First, theoretically ideal preconditioning strategies are considered, that is, preconditioners which are re-built on the basis of every single realization of the sampled coefficient. We consider different preconditioners and compare the average numbers of solver iterations with the case of

single constant preconditioners which are built on the basis of central measures of the variable coefficient. The effect of approximating the sampled realization $\kappa(\cdot, \theta)$ with $T(\hat{T}_m^{-1}\kappa(\cdot, \theta))$ is also investigated for different levels of truncations. Second, two-dimensional clustering experiments are conducted with different ratios λ_1/λ_2 . We investigate the effect of the choice of the map T_2 on the distribution and shape of the Voronoi cells of the stationary quantizer q_2 , as well as on the distribution of attribution frequencies. Third, the effect on the convergence behavior of the preconditioning strategies based on non-trivial Voronoi quantizers of the random variable coefficient is investigated. Finally, we briefly comment on an attempt to improve the proposed quantizers with local interpolations in a way which is similar to what was done in [60].

7.1. Experiments with theoretically ideal preconditioning strategies.

We consider the case where the random variable coefficient is sampled by Monte Carlo. For each realization $\kappa(\cdot, \theta)$, the corresponding matrix $\mathbf{A}(\theta)$ is used to define a SPD realization-dependent preconditioner $\mathbf{M}_\bullet(\theta)$ where \bullet indicates the type of preconditioner. Different types of preconditioners are considered, namely block-Jacobi (bJ) with 200 diagonal blocks, non-overlapping domain decomposition (DD) on the basis of finite element mesh partitions into 200 subdomains, and algebraic multi-grids (AMG). The DD preconditioner considered for this experiment is LORASC [25] without low rank correction. So it essentially consists of approximating the Schur complement with the boundary-to-boundary operator and apply it in the context of a preconditioner for the non-decomposed operator $\mathbf{A}(\theta)$. The AMG preconditioner we use is based on a single V-cycle with smoothed aggregation, just as proposed by default in [5]. These so-called theoretical ideal preconditioning strategies are compared to the case where a single constant preconditioner \mathbf{M}_\bullet is used for all realizations, built on the basis of $\mathbf{A}(0)$, i.e., the discretized operator obtained by setting the underlying Gaussian process G to its zero mean all over Ω . Then, the average number of PCG iterations to reach a backward error of 10^{-6} is estimated for different numbers of degrees of freedom (DoFs) of the discretization going from 4,000 to 128,000 by factors of 2. The results are presented in Fig. 1.

From Fig. 1, we can say that, irrespective of whether a constant preconditioner is preferred over re-building the preconditioner for every single realization, the average number of solver iterations is least sensitive to the number of DoFs when using AMG, followed by DD with bJ at last. The rates at which these average numbers of iterations increase as a function of the number of DoFs do not change whether a constant preconditioner is used or a realization-dependent approach is adopted. As expected for the case of an isotropic Poisson equation discretized with \mathbb{P}_1 finite elements, AMG offers the best convergence behavior, followed by DD and then bJ. We can also say that the ratio of solver iterations done when using a single constant preconditioner over the number of iterations done with a realization-dependent approach, does not significantly depend on the number of DoFs. A surprising observation is that, although AMG performs best on average, it shows the largest sensitivity of resorting to a constant preconditioner, yielding an approximate 10X increase of the number of solver iterations compared to using a realization-dependent approach. Those increases are about 3X and 2-3X when using DD and bJ, respectively. Therefore, not only AMG is the best preconditioner for the Poisson equation, but it also has the most to gain, relatively speaking, from defining alternative preconditioning strategies which tend to a realization-dependent approach.

A second experiment is conducted with a different type of theoretically ideal preconditioner, namely one that uses the quantizer $\tilde{q} : \kappa(\cdot, \theta) \mapsto T(\hat{T}_m^{-1}\kappa(\cdot, \theta))$. That is, a

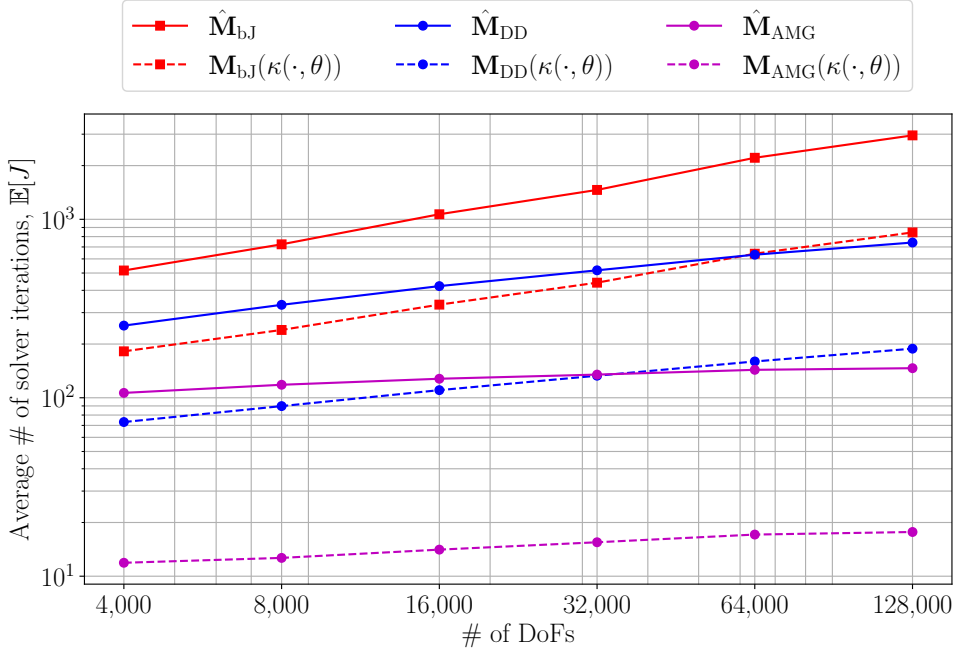


FIGURE 1. Scaling of the average number of solver iterations with respect to the number of DoFs using limit preconditioning strategies.

preconditioner $\mathbf{M}(T(\hat{T}_m^{-1}\kappa(\cdot, \theta)))$ is assembled on the basis of every single realization $\kappa(\cdot, \theta)$ of the random coefficient. For the case in which $\epsilon(\hat{T}_m^{-1}\kappa) \approx 0$, no distortion is induced by the quantization. Therefore, if $\mathbf{M}(T(\hat{T}_m^{-1}\kappa(\cdot, \theta)))$ is a factorization of $\mathbf{A}(\kappa(\cdot, \theta))$ then, in theory, only a single PCG iteration is necessary for the iterative solve. In practice, this approach makes no sense because it takes approximately as much effort to compute a factorization of $\mathbf{A}(\kappa(\cdot, \theta))$ as it takes to solve the linear system without preconditioner. If, however, we pick m such that $\epsilon(\hat{T}_m^{-1}\kappa) > 0$, a difference is induced between $\mathbf{A}(T(\hat{T}_m^{-1}\kappa(\cdot, \theta)))$ and $\mathbf{A}(\kappa(\cdot, \theta))$. Then, it is expected that the number of PCG iterations increases with $\epsilon(\hat{T}_m^{-1}\kappa)$. Using such a preconditioning strategy with $\epsilon(\hat{T}_m^{-1}\kappa) > 0$ is completely useless in practice since factorizing $\mathbf{A}(T(\hat{T}_m^{-1}\kappa(\cdot, \theta)))$ is a priori as difficult as factorizing $\mathbf{A}(\kappa(\cdot, \theta))$. However, for the case in which a non-trivial P -quantizer q of κ with a finite number P of preconditioners is considered, the dimension m of the underlying quantizer q_2 becomes an important feature, as will show in the results of Section 7.3. Also, for a given type of preconditioner, the performance of a strategy based on \tilde{q} can serve as a limit of comparison for strategies with less trivial Voronoi quantizers. Therefore, as a means to better understand the role of m on a preconditioning strategy, it is important to understand how the average number of solver iterations depends on m as well as on the related error $\epsilon(\hat{T}_m^{-1}\kappa)$ when using an ideal quantizer \tilde{q} . In Fig. 2, we show how the average number of PCG iterations evolve as a function of m and the relative energy $1 - \epsilon(\hat{T}_m^{-1}\kappa)$ of the underlying Gaussian process using both Cholesky factorization of $\mathbf{A}(T(\hat{T}_m^{-1}\kappa))$ and AMG preconditioners. The case considered is for a mesh with 200,332 elements and 100,652 DoFs yielding $n = 99,681$.

As expected, the results of Fig. 2 show that number of solver iterations decreases

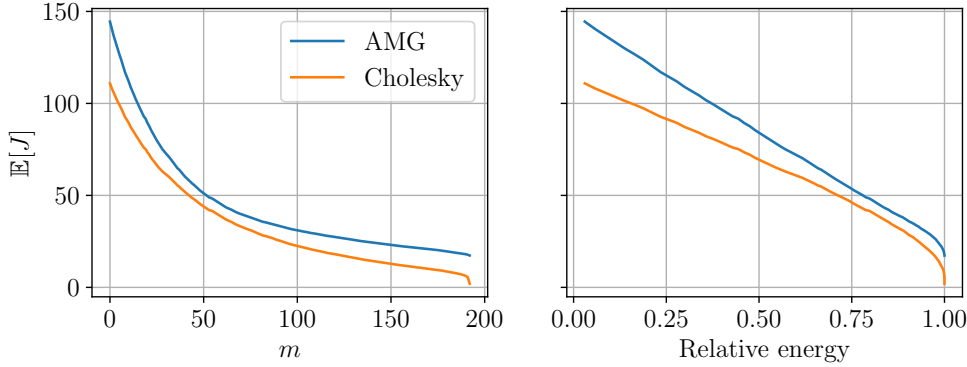


FIGURE 2. Average number of solver iterations J as a function of the number m of KL modes used for $\hat{T}_m^{-1}\kappa$ with a quantizer $\tilde{q} : \kappa(\cdot) \mapsto T(\hat{T}_m^{-1}\kappa(\cdot))$.

monotonically as m and the relative energy increase, irrespective of whether Cholesky factorizations or AMG preconditioners are used. We can see that the maximum difference of average number of solver iterations between the Cholesky factorizations and the AMG preconditioners occurs at $m = 0$, where it is of the order of 20%. This difference is smaller for all the other values of m . As such, we can tell that AMG is a very good preconditioner in that it provides average numbers of solver iterations which are close to what is obtained with Cholesky factorizations. We can see a clear dependence of the difference of average numbers of solver iterations between Cholesky factorizations and AMG preconditioners on the relative energy. As the relative energy approaches 1, i.e., as $\epsilon(\hat{T}_m^{-1}\kappa)$ vanishes, the difference of effect on convergence of the AMG preconditioners compared to the Cholesky factorizations decreases significantly. For most of the range of relative energy, the average number of solver iterations depends almost linearly on the relative energy.

7.2. Two-dimensional stationary quantizers. Here, we try to illustrate how the properties of the stationary vector quantizers q_2 depend on the choice of map T_2 as well as on the distribution of the eigenvalues $\lambda_1, \dots, \lambda_m$. Two choices of map T_2 were previously formulated in Section 6, and both are considered in this experiment. The distribution of $\lambda_1, \dots, \lambda_m$ depends strongly on the covariance function of $G(x, \theta)$, particularly on the correlation length, and the roughness in the more general case of Matérn covariance functions. Understanding the relation between the properties of the stationary quantizers q_2 and the distribution of $\lambda_1, \dots, \lambda_m$ can provide useful insights for other covariance functions. For purposes of illustration, we carry experiments with $m = 2$ and different values of the ratio λ_2/λ_1 so as to emulate the effect of the distribution of $\lambda_1, \dots, \lambda_m$ on the properties of the stationary quantizers q_2 .

For stationary quantizers q_2 obtained with $T_2^{-1}(\xi) := \mathbf{\Lambda}^{1/2}\xi$, Fig. 3 presents the Voronoi cells with their centers and normalized attribution frequencies $f_1^{(n_s)}, \dots, f_P^{(n_s)}$ for the quantization rates $P = 10, 100$ and 1,000 with a ratio $\lambda_2/\lambda_1 = 1, 0.1$ and 0.01. Similarly results are presented in Fig. 4 for the case in which $T_2^{-1}(\xi) := \mathbf{\Lambda}^{1/2}F_\xi \circ \xi$. In these experiments, the stationary vector quantizers are computed by k -means with a sample size $n_s = 100,000$. However, very similar results were obtained with the CLVQ algorithm.

From Fig. 3, we can see that the spatial distribution of centroids of the stationary

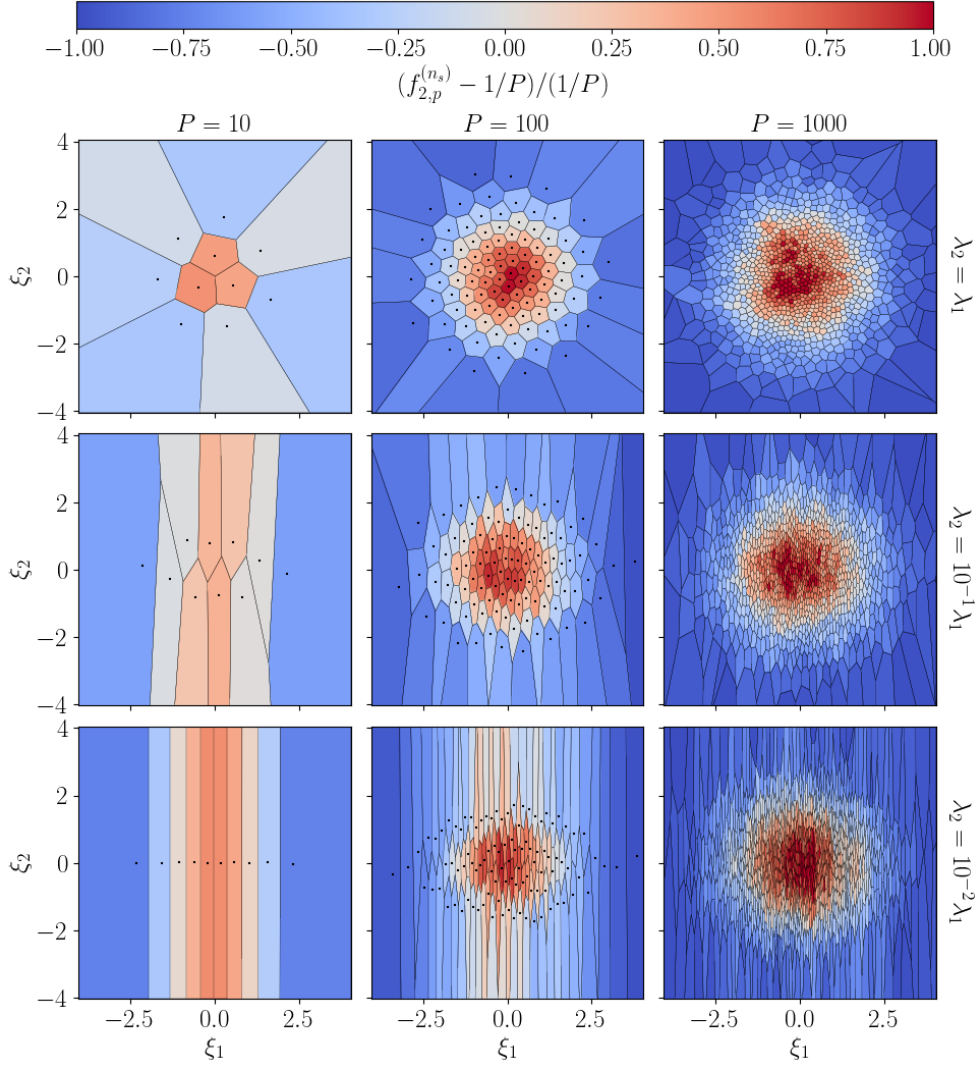


FIGURE 3. Attribution frequencies $f_{2,p}^{(n_s)}$ of the quantizer q_2 obtained by k -means with the map $T_2^{-1}(\xi) = \mathbf{\Lambda}^{1/2}\xi$ where $\xi \sim \mathcal{N}(\mathbf{0}, \mathbf{I}_2)$.

quantizer q_2 strongly depends on the ratio λ_2/λ_1 , and particularly so for the smaller values of P . For $\lambda_2/\lambda_1 = 1$ and $P = 10$, the centroids of q_2 form a circular cloud with two concentric rings of cells. The Voronoi cells located near the origin are small polygons with aspect ratios close to 1. The Voronoi cells located further from the origin are much larger and elongated as they indefinitely extend away from the origin. For the larger values of P , the circular shape of the cloud of centroids is preserved. Similarly as for $P = 10$, there are concentric rings of Voronoi cells, each with somewhat constant cell sizes. The size of these cells progressively increases as the distance of the centroid from the origin increases. For $\lambda_2/\lambda_1 = 0.1$ and $P = 10$, the centroids of q_2 form a nearly ellipsoidal cloud with the major axis along ξ_1 . The two Voronoi

cells whose centroids are at the extremities of the major axis extend indefinitely along ξ_1 away from the origin and in both the positive and negative directions of ξ_2 . All the other Voronoi cells whose centroids are closer to the origin are bounded on both sides along ξ_2 as well as near the center of ξ_1 while they extend indefinitely along ξ_1 away from the origin. For larger values of P , the centroids form clouds which are less and less elongated as P increases. All the Voronoi cells are elongated along ξ_2 , and increasingly so as the centroid is further from the origin. For $\lambda_2/\lambda_1 = 0.01$ and $P = 10$, the centroids of q_2 form a line along ξ_1 . The two Voronoi cells whose centroids are at the edges of the line extend indefinitely along ξ_1 away from the origin and in both the positive and negative directions along ξ_2 . All the other Voronoi cells whose centroids are closer to the origin are bounded on both sides along ξ_2 while they extend indefinitely along both the positive and negative directions of ξ_1 . Similarly as before, for larger values of P , the centroids form clouds which are less and less elongated as P increases. Again, all the Voronoi cells are increasingly elongated along ξ_2 as the centroids are further from the origin. Irrespective of the values of P and λ_2/λ_1 , the Voronoi cells whose centroid is near the origin have attribution frequencies which are significantly greater than $1/P$. These attribution frequencies keep decreasing as the distance of the centroid from the origin increases. All the Voronoi cells whose centroids are the most distant from the origin have attribution frequencies which are significantly smaller than $1/P$. By plotting these attribution frequencies, we can see that they vary in form of a bell curve as a function of the norm $\|\hat{\xi}_p\|_2$.

In Fig. 4, the spatial distribution of centroids of the stationary quantizer q_2 also depends on the ratio λ_2/λ_1 for $P = 10$. For $\lambda_2/\lambda_1 = 1$ and $P = 10$, the centroids of q_2 form a square cloud made of three parallel horizontal lines. A Voronoi cell has its centroid located almost exactly at the origin. This cell is small with an aspect ratio close to 1. There are narrow Voronoi cells which start at each of the edges of the central cell and extend indefinitely away from those edges. The tessellation is completed by four large square cells at the corners of the square cloud of centroids. For larger values of P , the shape of the centered square cloud of centroids is preserved. Similarly as for $P = 10$, there are four large square cells at the corners of the square cloud of centroids. In the center of the cloud, there are multiple small Voronoi cells with aspect ratios close to 1. All along the edges of the cloud of centroids and between the four large square cells, there are multiple narrow cells which extend indefinitely away from the edges of the square cloud of centroids. For $\lambda_2/\lambda_1 = 0.1$ and $P = 10$, the centroids of q_2 form a rectangular cloud made of two parallel horizontal lines. Once again, there are four large Voronoi cells at the corners of the cloud of centroids. All the other cells are narrowly trapped between the large square cells, they span indefinitely away from the ξ_1 axis. For larger values of P , the centroids still form a rectangular cloud. The center of the cloud of centroids is also packed with very small cells with aspect ratios close to 1. All along the edges of the rectangular cloud of cells, there are narrow cells which extend indefinitely away from the edges. There are more of these cells on the top and bottom edges than there are on the left and right edges. For $\lambda_2/\lambda_1 = 0.01$ and $P = 10$, the centroids of q_2 form a line along ξ_1 . The two Voronoi cells whose centroids are at the edges of the line extend indefinitely along ξ_1 away from the origin and in both the positive and negative directions along ξ_2 . All the other Voronoi cells whose centroids are closer to the origin are bounded on both sides along ξ_2 while they extend indefinitely along both the positive and negative directions of ξ_1 . For larger values of P , the centroids form a rectangular cloud with the longer edges along ξ_1 . The center of the cloud of centroids is packed with very small cells. Again, all along

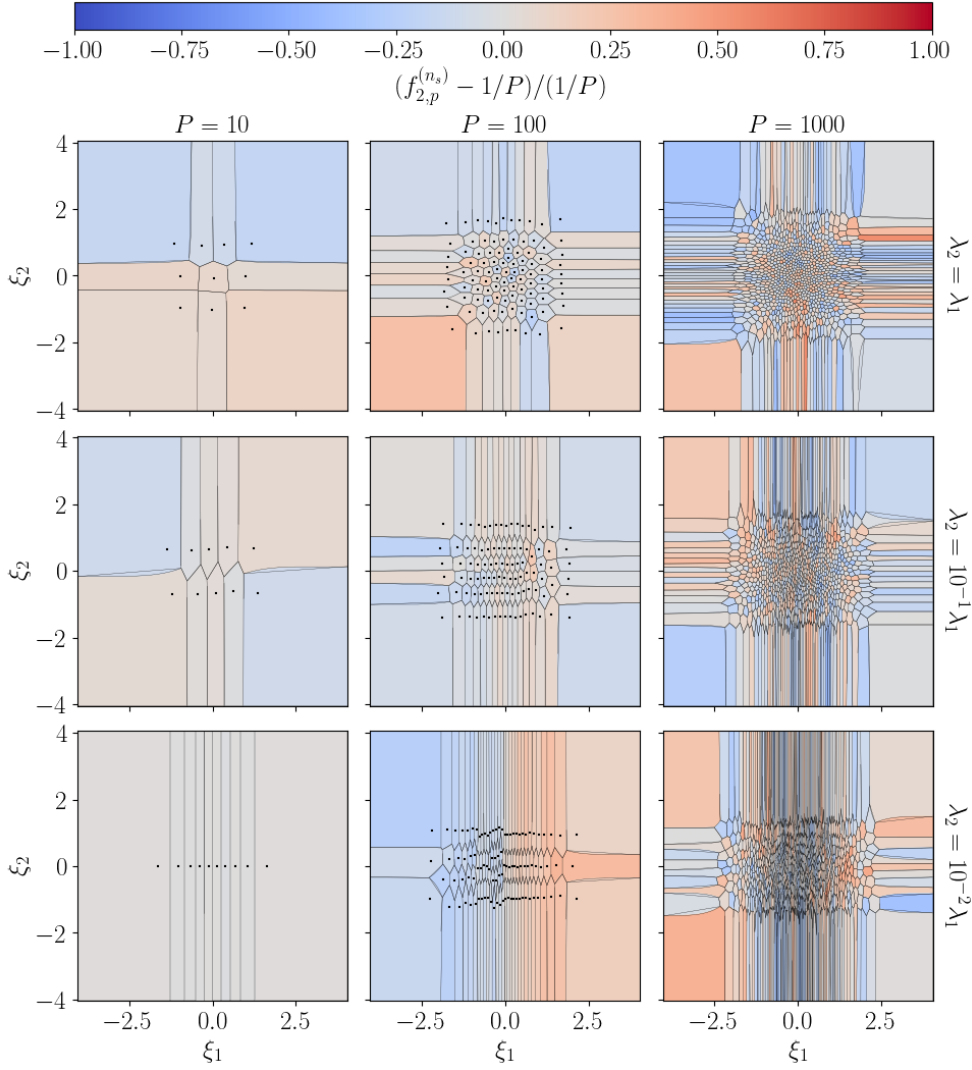


FIGURE 4. Attribution frequencies $f_{2,p}^{(n_s)}$ of the quantizer q_2 obtained by k -means with the map $T_2^{-1}(\xi) = \mathbf{\Lambda}^{1/2}F_\xi \circ \xi$ where $\xi \sim \mathcal{N}(\mathbf{0}, \mathbf{I}_2)$.

the edges of the rectangular cloud of centroids, there are narrow cells which span indefinitely away from the edges. There are significantly more of these cells on the top and bottom edges than there are on the left and right edges. Irrespective of the values of P and λ_2/λ_1 , all the Voronoi cells have attribution frequencies close to $1/P$. There is no discernible spatial pattern of how the attribution frequencies deviate from $1/P$.

7.3. Performance of preconditioning strategies based on Voronoi quantizers. In Fig. 5, we consider the preconditioning strategies based on stationary quantizers q_2 for the two possible choices of T_2 and we present the effect on (i) the average number of solver iterations per preconditioner as well as on (ii) the number of linear

systems solved per preconditioner, and (iii) the cumulated number of solver iterations per preconditioner. These quantities are presented in scatter plots as functions of the distance $\|\hat{\xi}_p\|$ of the centroid $\hat{\xi}_p$ to the origin. The results presented are obtained for an approximating variable coefficient composed of $m = 8$ KL modes for a quantization with $P = 1,000$ preconditioners. The preconditioners used are AMG, and the Monte Carlo simulation consists of 100,000 realizations. Once again, we consider the mesh with 200,332 elements so that $n = 99,681$. First, we can say that, irrespective of T_2 , there is some level of linear correlation between $\mathbb{E}_p[J]$ and $\|\hat{\xi}_p\|$. It is actually surprising that these quantities are not more correlated. Indeed, our experiments have shown that the conditioning of a Galerkin operator $\mathbf{A}(\kappa(\cdot, \hat{\xi}_p))$ tends to increase with the norm $\|\hat{\xi}_p\|$ of the latent variable $\hat{\xi}_p$ of the underlying coefficient $\kappa(\cdot, \hat{\xi}_p)$. Second, we can see that, when using $T_2^{-1}(\xi) = \Lambda^{1/2}\xi$, the number n_p of linear systems solved with a preconditioner $\hat{\mathbf{M}}_p$ is rather strongly correlated with the size of the norm $\|\hat{\xi}_p\|$. This result is not surprising when we consider the dependence of the attribution frequency $f_{2,p}^{(n_s)}$ on the distance $\|\hat{\xi}_p\|$ presented in Section 7.2 for $m = 2$. In particular, the number n_p of linear systems solved decreases with $\|\hat{\xi}_p\|$. We can see that choosing $T_2^{-1}(\xi) = \Lambda^{1/2}\xi$ leads to a larger spread of the possible values taken by n_p than when using $T_2^{-1}(\xi) = \Lambda^{1/2}F_\xi \circ \xi$. In the case $T_2^{-1}(\xi) = \Lambda^{1/2}F_\xi \circ \xi$, the number n_p of linear systems solved per preconditioner does not strongly correlate with $\|\hat{\xi}_p\|$. Third, the scatter plot of the cumulated number of solver iterations as a function of the norm $\|\hat{\xi}_p\|$ strongly resembles the scatter plot of n_p . Hence, the number of cumulated solver iterations strongly correlates with $\|\hat{\xi}_p\|$ when using $T_2^{-1}(\xi) = \Lambda^{1/2}\xi$. On the other hand, using $T_2^{-1}(\xi) = \Lambda^{1/2}F_\xi \circ \xi$ leads to less spread of the number of cumulated solver iterations. In other words, the computational load is more balanced in the latter case. Although the figure is not presented here, similar results as those of Fig. 5 were obtained using Cholesky factorizations in place of AMG preconditioners. The results are almost identically the same, which is why we do not present them here, with the exception that all the average and cumulated numbers of solver iterations are slightly smaller.

In Fig. 6, we present the overall average number of solver iterations for each of the three preconditioning strategies presented in this chapter. That is, the two strategies based on stationary quantizers q_2 built with different choices of T_2 , but also the strategy built with deterministic grids (see Section 5). In the case of the stationary quantizers, the results are presented for different numbers m of KL modes used for the approximating coefficient. These values of m are selected so as to correspond to relative energies which properly cover the whole range from 0 to 1. In particular, we use $m = 8$ which corresponds to approximately 20% of relative energy as well as $m = 24$ (50%), $m = 48$ (75%) and $m = 170$ (99%). Different numbers P of preconditioners are considered, namely $P = 1, 10, 100, 1,000$ and $10,000$. When it comes to the preconditioning strategy based on deterministic grids, all the possible numbers of preconditioners from $P = 1$ to $P = 8,193$ are considered, i.e., we used $P = 1 + 2^m$ for $m = 1, \dots, 13$ and $P = 1$ for $m = 0$. For the preconditioning strategies based on stationary quantizers, the relation between $\mathbb{E}[J]$ and the number P of preconditioners is fairly similar irrespective of T_2 , with the exception that for a given pair (m, P) , using $T_2^{-1}(\xi) = \Lambda^{1/2}F_\xi \circ \xi$ yields slightly larger values of $\mathbb{E}[J]$ than using $T_2^{-1}(\xi) = \Lambda^{1/2}\xi$. Besides this difference, the same phenomenon can be observed, irrespective of T_2 . That is, for $m = 8$, $\mathbb{E}[J]$ decreases as a function of P , at a decreasing rate as $\mathbb{E}[J]$ starts to stagnate for larger values of P . Using

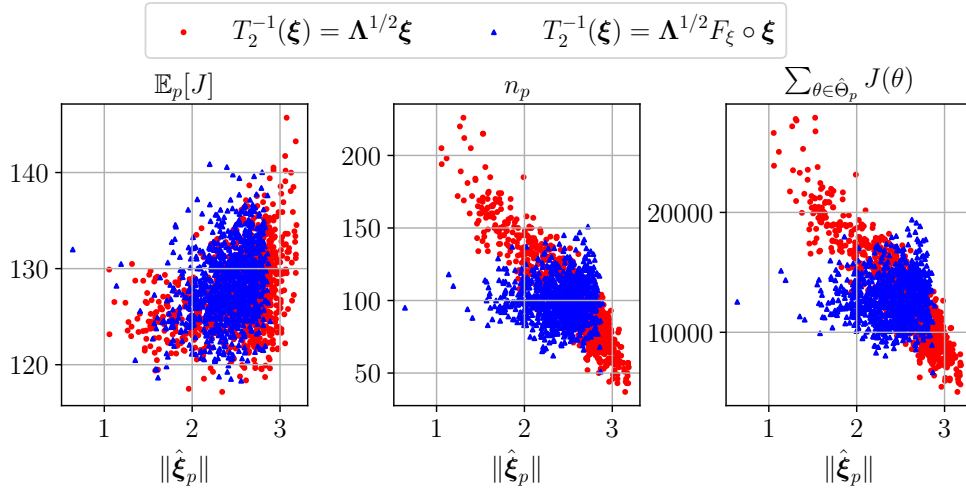


FIGURE 5. Average numbers of solver iterations, numbers of linear systems solved and total numbers of solver iterations per preconditioner. Number of KL modes $m = 8$. Number of preconditioners $P = 1,000$. Results obtained with AMG preconditioners.

$m = 8$ seems optimal for the smallest number of preconditioners considered, that is, $P = 10$. Similarly, for $m = 24$, $\mathbb{E}[J]$ decreases as a function of P , also at a decreasing rate, but stagnation starts occurring for larger values of P . Meanwhile, selecting $m = 24$ seems optimal when using $P = 100$ preconditioners. The same type of behavior is observed for $m = 48$, with the difference that $\mathbb{E}[J]$ is larger than when using smaller values of m for the smaller values P . Eventually, a stagnation also starts occurring, but for larger values of P . Using $m = 48$ is optimal when using $P = 100$ preconditioners. Finally, for $m = 170$, the stagnation is not captured for our investigated numbers P of preconditioners. Using $m = 170$ however does not as strongly impact $\mathbb{E}[J]$ as using smaller values of m in the case of $P = 10, 100$ and $1,000$. The choice $m = 170$ is optimal for $P = 10,000$ preconditioners. A major difference of the preconditioning strategy based on deterministic grids is that the number m of approximating KL modes depends on P . A consequence of this scheme on the evolution of the average number of solver iterations is that the decrease of $\mathbb{E}[J]$ does not stagnate as P is increased, unlike the case of the preconditioning strategies based on stationary quantizers with a fixed value of m . Meanwhile, although the preconditioning strategy based on deterministic grids does not necessarily yield values of $\mathbb{E}[J]$ as low as using a stationary quantizers with $T_2^{-1}(\xi) = \Lambda^{1/2}\xi$ with an optimally selected value of m , it does reasonably well for the entire range of values for the number P of preconditioners considered in this study.

7.4. Effect of local interpolation. Monte Carlo simulations with a quantized preconditioner are embarrassingly parallelizable on distributed computers, in which case each node stores only some of the preconditioners \mathbf{M}_p . Assuming that a node stores more than one preconditioner, we want to leverage all these *local* preconditioners so as to try and further improve the preconditioning of the system. This can be done using an interpolation of the preconditioner realization $\mathbf{M}(\theta)$ via an optimal projection in the linear span of the local preconditioners. Such an approach, which is

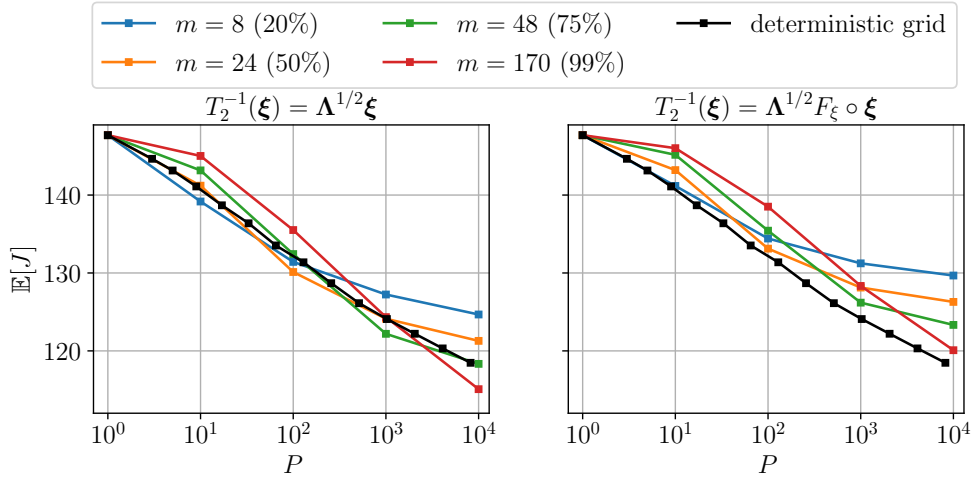


FIGURE 6. Average numbers of PCG iterations for different quantizations of preconditioners.

an adaptation of the work of Zahm and Nouy [60], was presented in Section 4.6 of [57] in complement of Voronoi quantizers. Experiments are conducted to test this strategy on the convergence behavior of PCG. As a means to build such local interpolations, groups of centroids must be formed. We do so using the k -means algorithm to find clusters of close centroids for every given quantization. For a given number P of preconditioners, we need to pick a number $M \leq P$ of clusters. We do so so as to have an average cluster size of 4. That is, for $P = 100, 1,000$ and $10,000$, we use $M = 25, 250$ and $2,500$, respectively. We develop local interpolators for the preconditioning strategies based on stationary quantizers for both choices of T_2 . We compute the coefficients of the local interpolation using the a random sketch of the matrix $\mathbf{A}(\theta)$. Similarly as in [60], we use matrix-free sub-sampled randomized Hadamard transforms. The experiment is conducted with AMG preconditioners as well as with Cholesky factorizations. However, for the totality of the linear systems solved, using a local interpolator shows absolutely no impact whatsoever on the number of solver iterations compared to using a single preconditioner \hat{M}_p . Another interpolation method described in the work of Zahm and Nouy [60] is used, namely the Shepard interpolation. Similarly, absolutely no impact is observed on the convergence of PCG.

8. Conclusion. We developed preconditioning strategies based on the quantization of random coefficient for the iterative solve of linear systems which arise from the discretization of stochastic elliptic PDEs for specific realizations of random variable coefficients which typically occur during Monte Carlo simulations. The problem of functional quantization of the random coefficient was transformed to a problem of vector quantization in the stochastic space induced by the KL expansion of a mapping $T^{-1}\kappa$ of the coefficient. From thereon, an additional map T_2 was introduced so as to allow some flexibility in the design of the vector quantizer q_2 which can be related to a quantizer of the coefficient field through Eq. (3.10). In particular, we considered Voronoi stationary quantizers which minimize the $L^2(\Omega)$ -distortion induced by the quantizer $\hat{P}_m^{\rightarrow} \circ T_2 \circ q_2 \circ T_2^{-1} \circ \hat{P}_m^{\leftarrow}$ of $\hat{T}_m^{-1}\kappa$. Two methods were considered to compute these stationary quantizers, namely k -means and CLVQ. In [45], it is argued that

k -means is untractable in multiple dimensions, i.e., when m becomes large. Hence, we compared the use of CLVQ to the use of k -means to compute stationary vector quantizers of $T_2^{-1}(\boldsymbol{\xi})$ where $\boldsymbol{\xi}$ is an m -dimensional standard Gaussian random vector with covariance \mathbf{I}_m . Experiments were conducted with both $T_2^{-1}(\boldsymbol{\xi}) = \boldsymbol{\Lambda}^{1/2}\boldsymbol{\xi}$ and $T_2^{-1}(\boldsymbol{\xi}) = \boldsymbol{\Lambda}^{1/2}F_\xi \circ \boldsymbol{\xi}$ where $\boldsymbol{\Lambda} = \text{diag}(\lambda_1, \dots, \lambda_m)$ in which $\lambda_1, \dots, \lambda_m$ are the dominant eigenvalues of the KL expansion of a stationary Gaussian process with unit variance and squared exponential covariance. Contrarily to what is claimed in [45], we had no difficulty computing stationary quantizers with comparable levels of distortion using both methods with values of m going up to 200 for numbers of clusters spanning from $P = 10$ to $P = 10,000$ with sample sizes of 100,000. When it comes to running times, CLVQ was faster for $P = 10$ while k -means was faster for $P = 1,000$ and 10,000. Note that the clustering of the latent random vectors to compute stationary quantizers is only a pre-processing phase of the Monte Carlo simulation which, for sufficiently large numbers of realizations, only represents a negligible fraction of the total computing effort. The great majority of the computational load is the iterative solve of the multiple linear systems corresponding to all the sampled realizations of the coefficient field.

We investigated the effect of the choice of the map T_2 on the properties of the stationary quantizer q_2 . It was shown that choosing $T_2^{-1}(\boldsymbol{\xi}) = \boldsymbol{\Lambda}^{1/2}\boldsymbol{\xi}$ leads to ellipsoidal clouds of centroids with aspect ratios depending on the distribution of $\lambda_1, \dots, \lambda_m$. The distribution of eigenvalues also impacts the shape of the Voronoi cells of the quantizer, whose sizes increase with the distance from the centroid of the cell to the origin. The attribution frequency $f_{2,p}^{(n_s)}$ also depends on the norm $\|\hat{\boldsymbol{\xi}}_p\|$ of the cell centroid in a way somewhat similar to a half bell curve. Meanwhile, using $T_2^{-1}(\boldsymbol{\xi}) = \boldsymbol{\Lambda}^{1/2}F_\xi \circ \boldsymbol{\xi}$ leads to rectangular clouds of centroids with aspect ratios which depend on the distribution of $\lambda_1, \dots, \lambda_m$. The distribution of eigenvalues does not significantly impact the shape of the Voronoi cells within the rectangular cloud, which all are very small. Systematically, some square Voronoi cells occur at the corners of the cloud of centroids, between which are packed elongated cells. The attribution frequency $f_{2,p}^{(n_s)}$ only slightly varies around the value $1/P$ without following any specific pattern with respect to the location of the centroid. The distribution of the attribution frequencies can be interpreted in terms of its effect on the underlying preconditioning strategy. For, $T_2^{-1}(\boldsymbol{\xi}) = \boldsymbol{\Lambda}^{1/2}F_\xi \circ \boldsymbol{\xi}$, the somewhat uniform distribution of $f_{2,1}^{(n_s)}, \dots, f_{2,P}^{(n_s)}$ with low spread around $1/P$ means that the underlying strategy is such that every preconditioner is used for approximately as many linear systems. On the other hand, the dependence of the attribution frequency on the norm $\|\hat{\boldsymbol{\xi}}_p\|$ which we observe when using $T_2^{-1}(\boldsymbol{\xi}) = \boldsymbol{\Lambda}^{1/2}\boldsymbol{\xi}$ is such that the preconditioners which correspond to smaller values of $\|\hat{\boldsymbol{\xi}}_p\|$ are used to solve more linear systems. Note that, typically, the conditioning number of a Galerkin operator increases with the norm of the latent vector $[\xi_1, \xi_2, \dots]$ which defines the realization of the underlying field $T^{-1}\kappa$.

In this work, we considered linear systems of dimension up to $n \approx 128,000$. Consequently, we were not able to simultaneously store all the preconditioners in memory for some values of P , i.e., 1,000 and 10,000. In practice, even larger linear systems may have to be solved, in which case only one or a couple of preconditioners may be stored in memory at once. Then, two possible ways to carry a Monte Carlo simulation arise. First, a sequential simulation relies on a preliminary step which consists of sampling all the latent random vectors of the simulation and attributing them to the corresponding centroids. These realizations are stored on disk. Then, we

start by loading the first preconditioner in memory as well as all the corresponding realizations. While the preconditioner is stored in memory, we assemble the linear system of each realization and solve each linear system. Once all the corresponding linear systems have been solved, it is time to load the second preconditioner in memory along with its corresponding realization, and so on. The second approach is parallel. Typically, one has access to a distributed computer. Then, one can identify a main node which is used to sample realizations of the random coefficient which are sent to the node with the corresponding preconditioner. In order to account for the total running time of a sequential simulation, one can simply look at the expected number of solver iterations of a given preconditioning strategy. Meanwhile, the total time of a parallel simulation is rather accounted by the maximum time taken by any of the nodes to solve all its attributed linear systems. Therefore, in the case of parallel simulations, we are also interested in the distribution of cumulated solver iterations among preconditioners for a given simulation.

For the case of parallel simulations, the preconditioning strategies based on stationary quantizers were considered for both choices of the map T_2 . It was observed that choosing $T_2^{-1}(\xi) = \mathbf{\Lambda}^{1/2}\xi$ leads to a larger spread of the number of cumulated solver iterations among the different preconditioners. Although the minimum number of cumulated solver iterations for a preconditioner is smaller with this choice of T_2 than when choosing $T_2^{-1}(\xi) = \mathbf{\Lambda}^{1/2}F_\xi \circ \xi$, so is the maximum number of cumulated solver iterations. Hence, we can say that $T_2^{-1}(\xi) = \mathbf{\Lambda}^{1/2}F_\xi \circ \xi$ leads to more balanced numbers of cumulated solver iterations and should thus be preferred for parallel simulations.

For the case of sequential simulations, the performance of a given preconditioning strategy can be evaluated in terms of the average number of solver iterations. Once again, preconditioning strategies were considered which are based on stationary quantizers based on the two possible choices of the map T_2 . It was observed that choosing $T_2^{-1}(\xi) = \mathbf{\Lambda}^{1/2}\xi$ leads to smaller average numbers of solver iterations and should thus be preferred for sequential simulations. However, the optimal choice of the number m of KL modes of the approximating coefficient field was shown to depend on the number P of preconditioners. That is, for smaller values of P , it is preferable to chose a dimension m of the approximating stochastic space which is rather small. However, as we increase the value of P , the same choice m is such that the stochastic space starts to saturate with centroids and the effect on the convergence of PCG starts to be less significant, in which case it is advantageous to increase the dimension m . Hence, in order to chose the optimal number m for given number P of preconditioners, one may have to run a preliminary study in which the relative performance of different values of m is investigated. A third preconditioning strategy based on deterministic grids was shown to provide a reasonable alternative to the strategies based on stationary quantizers. Indeed, the increase of the dimension m of the approximating stochastic space of the deterministic grid as a function of the number P of preconditioners is such that the strategy based on deterministic grids never seems to saturate as opposed to the strategies based on stationary quantizers with a fixed value of m . Meanwhile, the average numbers of solver iterations achieved by the strategy based on deterministic grids are also reasonably small.

Local interpolations of preconditioners were considered as an attempt to leverage the fact that, even when using distributed computers, each node is likely able to store more than one preconditioner. Therefore, local interpolations based on the optimal linear span of preconditioners from small clusters of neighboring centroids were used

in a similar way to what was proposed in [60]. This strategy was however shown to not bring any improvement to our different strategies based on quantizers of random coefficients. Overall, the resort to Voronoi quantizers allowed to decrease the average number of solver iterations by up to 1.25X when using 10,000 preconditioners in comparison to a strategy with a constant AMG preconditioner. However, it was shown that a realization-dependent preconditioning strategy enables a near 10X decrease of the average number of solver iterations for AMG. That is, Voronoi quantizers with up to 10,000 preconditioners can reach only up to 12.5% of the speedup theoretically achievable by a realization-dependent approach. This rather disappointing figure should serve as a motivation to deploy further efforts to develop even better preconditioning strategies aimed at solving stochastic PDEs. Given the high relative speedup achievable for AMG, it seems particularly relevant to try and build stochastic multigrid preconditioners which make use of the KL representation of the random coefficient.

REFERENCES

- [1] I. BABUŠKA, F. NOBILE, AND R. TEMPONE, A stochastic collocation method for elliptic partial differential equations with random input data, *SIAM Journal on Numerical Analysis*, 45 (2007), pp. 1005–1034.
- [2] A. BANERJEE, S. MERUGU, I. S. DHILLON, AND J. GHOSH, Clustering with Bregman divergences, *Journal of machine learning research*, 6 (2005), pp. 1705–1749.
- [3] J. BECK, F. NOBILE, L. TAMELLINI, AND R. TEMPONE, Convergence of quasi-optimal stochastic Galerkin methods for a class of PDEs with random coefficients, *Computers & Mathematics with Applications*, 67 (2014), pp. 732–751.
- [4] J. BECK, R. TEMPONE, F. NOBILE, AND L. TAMELLINI, On the optimal polynomial approximation of stochastic PDEs by Galerkin and collocation methods, *Mathematical Models and Methods in Applied Sciences*, 22 (2012), p. 1250023.
- [5] W. BELL, L. OLSON, AND J. SCHRODER, PyAMG: Algebraic multigrid solvers in Python v2.0, <http://www.pyamg.org>, (2011).
- [6] A. BENVENISTE, M. MÉTIVIER, AND B. PRIOURET, Algorithmes adaptatifs et approximations stochastiques, collection techniques stochastiques, 1987.
- [7] G. BLATMAN AND B. SUDRET, Adaptive sparse polynomial chaos expansion based on least angle regression, *Journal of computational Physics*, 230 (2011), pp. 2345–2367.
- [8] L. M. BREGMAN, The relaxation method of finding the common point of convex sets and its application to the solution of problems in convex programming, *USSR computational mathematics and mathematical physics*, 7 (1967), pp. 200–217.
- [9] L. BRUN AND M. MOKHTARI, Two high speed color quantization algorithms, in *Proceedings of the 1st international conference on color in graphics and image processing*, 2000, pp. 116–121.
- [10] R. E. CAFLISCH, Monte Carlo and quasi-Monte Carlo methods, *Acta numerica*, 7 (1998), pp. 1–49.
- [11] M. E. CELEBI, Improving the performance of k -means for color quantization, *Image and Vision Computing*, 29 (2011), pp. 260–271.
- [12] A. CHKIFA, A. COHEN, AND C. SCHWAB, High-dimensional adaptive sparse polynomial interpolation and applications to parametric PDEs, *Foundations of Computational Mathematics*, 14 (2014), pp. 601–633.
- [13] K. A. CLIFFE, M. B. GILES, R. SCHEICHL, AND A. L. TECKENTRUP, Multilevel Monte Carlo methods and applications to elliptic PDEs with random coefficients, *Computing and Visualization in Science*, 14 (2011), pp. 3–15.
- [14] P. R. CONRAD AND Y. M. MARZOUK, Adaptive Smolyak pseudospectral approximations, *SIAM Journal on Scientific Computing*, 35 (2013), pp. A2643–A2670.
- [15] P. G. CONSTANTINE, M. S. ELDERED, AND E. T. PHIPPS, Sparse pseudospectral approximation method, *Computer Methods in Applied Mechanics and Engineering*, 229 (2012), pp. 1–12.
- [16] M. K. DEB, I. M. BABUŠKA, AND J. T. ODEN, Solution of stochastic partial differential equations using Galerkin finite element techniques, *Computer Methods in Applied Mechanics and Engineering*, 190 (2001), pp. 6359–6372.
- [17] H. C. ELMAN AND T. SU, A low-rank multigrid method for the stochastic steady-state diffusion

- problem, *SIAM Journal on Matrix Analysis and Applications*, 39 (2018), pp. 492–509.
- [18] A. FISCHER, Quantization and clustering with Bregman divergences, *Journal of Multivariate Analysis*, 101 (2010), pp. 2207–2221.
- [19] P. FRAUENFELDER, C. SCHWAB, AND R. A. TODOR, Finite elements for elliptic problems with stochastic coefficients, *Computer methods in applied mechanics and engineering*, 194 (2005), pp. 205–228.
- [20] B. A. FRIGYIK, S. SRIVASTAVA, AND M. R. GUPTA, Functional Bregman divergence and Bayesian estimation of distributions, *IEEE Transactions on Information Theory*, 54 (2008), pp. 5130–5139.
- [21] A. GERSHO AND R. M. GRAY, Vector quantization and signal compression, vol. 159, Springer Science & Business Media, 2012.
- [22] M. GERVAUTZ AND W. PURGATHOFER, A simple method for color quantization: Octree quantization, in *New trends in computer graphics*, Springer, 1988, pp. 219–231.
- [23] R. G. GHANEM AND P. D. SPANOS, Stochastic finite elements: a spectral approach, Courier Corporation, 2003.
- [24] S. GRAF AND H. LUSCHGY, Foundations of quantization for probability distributions, Springer, 2007.
- [25] L. GRIGORI, F. NATAF, AND S. YOUSEF, Robust algebraic Schur complement preconditioners based on low rank corrections, PhD thesis, Inria, 2014.
- [26] M. R. HESTENES, E. STIEFEL, ET AL., Methods of conjugate gradients for solving linear systems, *Journal of research of the National Bureau of Standards*, 49 (1952), pp. 409–436.
- [27] J. KIEFFER, Exponential rate of convergence for Lloyd’s method I, *IEEE Transactions on Information Theory*, 28 (1982), pp. 205–210.
- [28] O. M. KNIO AND O. LE MAITRE, Uncertainty propagation in CFD using polynomial chaos decomposition, *Fluid dynamics research*, 38 (2006), p. 616.
- [29] T. KOHONEN, Learning vector quantization, in *Self-organizing maps*, Springer, 1995, pp. 175–189.
- [30] T. LALOË, L1-quantization and clustering in Banach spaces, *Mathematical Methods of Statistics*, 19 (2010), pp. 136–150.
- [31] O. LE MAITRE, O. KNIO, B. DEBUSSCHERE, H. NAJM, AND R. GHANEM, A multigrid solver for two-dimensional stochastic diffusion equations, *Computer Methods in Applied Mechanics and Engineering*, 192 (2003), pp. 4723–4744.
- [32] O. LE MAITRE AND O. M. KNIO, Spectral methods for uncertainty quantification: with applications to computational fluid dynamics, Springer Science & Business Media, 2010.
- [33] O. P. LE MAITRE, M. T. REAGAN, H. N. NAJM, R. G. GHANEM, AND O. M. KNIO, A stochastic projection method for fluid flow: II. random process, *Journal of computational Physics*, 181 (2002), pp. 9–44.
- [34] K. LEE AND H. C. ELMAN, A preconditioned low-rank projection method with a rank-reduction scheme for stochastic partial differential equations, *SIAM Journal on Scientific Computing*, 39 (2017), pp. S828–S850.
- [35] T. LINDER, Learning-theoretic methods in vector quantization, in *Principles of nonparametric learning*, Springer, 2002, pp. 163–210.
- [36] J. S. LIU AND J. S. LIU, Monte Carlo strategies in scientific computing, vol. 75, Springer, 2001.
- [37] S. LLOYD, Least squares quantization in PCM, *IEEE transactions on information theory*, 28 (1982), pp. 129–137.
- [38] G. J. LORD, C. E. POWELL, AND T. SHARDLOW, An introduction to computational stochastic PDEs, vol. 50, Cambridge University Press, 2014.
- [39] J. MACQUEEN, Classification and analysis of multivariate observations, in *5th Berkeley Symp. Math. Statist. Probability*, 1967, pp. 281–297.
- [40] H. N. NAJM, Uncertainty quantification and polynomial chaos techniques in computational fluid dynamics, *Annual review of fluid mechanics*, 41 (2009), pp. 35–52.
- [41] F. NOBILE, R. TEMPONE, AND C. G. WEBSTER, A sparse grid stochastic collocation method for partial differential equations with random input data, *SIAM Journal on Numerical Analysis*, 46 (2008), pp. 2309–2345.
- [42] A. NOUY, A generalized spectral decomposition technique to solve a class of linear stochastic partial differential equations, *Computer Methods in Applied Mechanics and Engineering*, 196 (2007), pp. 4521–4537.
- [43] A. NOUY, Generalized spectral decomposition method for solving stochastic finite element equations: invariant subspace problem and dedicated algorithms, *Computer Methods in Applied Mechanics and Engineering*, 197 (2008), pp. 4718–4736.
- [44] A. NOUY AND O. P. LE MAITRE, Generalized spectral decomposition for stochastic nonlinear

- problems, *Journal of computational physics*, 228 (2009), pp. 202–235.
- [45] G. PAGÈS, A space quantization method for numerical integration, *Journal of computational and applied mathematics*, 89 (1998), pp. 1–38.
- [46] G. PAGÈS AND J. PRINTEMS, Optimal quadratic quantization for numerics: the Gaussian case, *Monte Carlo methods and applications*, 9 (2003), pp. 135–165.
- [47] C. C. PAIGE AND M. A. SAUNDERS, Solution of sparse indefinite systems of linear equations, *SIAM journal on numerical analysis*, 12 (1975), pp. 617–629.
- [48] M. PAPADRAKAKIS AND V. PAPADOPOULOS, Robust and efficient methods for stochastic finite element analysis using Monte Carlo simulation, *Computer methods in applied mechanics and engineering*, 134 (1996), pp. 325–340.
- [49] C. E. POWELL AND H. C. ELMAN, Block-diagonal preconditioning for spectral stochastic finite-element systems, *IMA Journal of Numerical Analysis*, 29 (2009), pp. 350–375.
- [50] M. T. REAGANA, H. N. NAJM, R. G. GHANEM, AND O. M. KNIO, Uncertainty quantification in reacting-flow simulations through non-intrusive spectral projection, *Combustion and flame*, 132 (2003), pp. 545–555.
- [51] J. F. REIS, O. P. LE MAÎTRE, P. M. CONGEDO, AND P. MYCEK, Stochastic preconditioning of domain decomposition methods for elliptic equations with random coefficients, *Computer Methods in Applied Mechanics and Engineering*, 381 (2021), p. 113845.
- [52] Y. SAAD, Iterative methods for sparse linear systems, vol. 82, SIAM, 2003.
- [53] Y. SAAD AND M. H. SCHULTZ, GMRES: A generalized minimal residual algorithm for solving nonsymmetric linear systems, *SIAM Journal on scientific and statistical computing*, 7 (1986), pp. 856–869.
- [54] M. SABIN AND R. GRAY, Global convergence and empirical consistency of the generalized Lloyd algorithm, *IEEE Transactions on information theory*, 32 (1986), pp. 148–155.
- [55] H. STEINHAUS ET AL., Sur la division des corps matériels en parties, *Bull. Acad. Polon. Sci*, 1 (1956), p. 801.
- [56] L. TAMELLINI, O. LE MAITRE, AND A. NOUY, Model reduction based on proper generalized decomposition for the stochastic steady incompressible Navier–Stokes equations, *SIAM Journal on Scientific Computing*, 36 (2014), pp. A1089–A1117.
- [57] N. VENKOVIC, Preconditioning strategies for stochastic elliptic partial differential equations, PhD thesis, Université de Bordeaux, 2023.
- [58] M. VERLEYSSEN, Les principaux modèles de réseaux de neurones artificiels, in *Les réseaux de neurones en finance: conception et applications*, 1995.
- [59] Z. XIANG, Color image quantization by minimizing the maximum intercluster distance, *ACM Transactions on Graphics (TOG)*, 16 (1997), pp. 260–276.
- [60] O. ZAHM AND A. NOUY, Interpolation of inverse operators for preconditioning parameter-dependent equations, *SIAM Journal on Scientific Computing*, 38 (2016), pp. A1044–A1074.